Water SA 51(4) 337–351 / Oct 2025
https://doi.org/10.17159/wsa/2025.v51.i4.4119

Research paper

Assessing groundwater potential using GIS-MCDM and remote sensing techniques: A case study of Franschhoek, South Africa

C Musekiwa[1], C Penn-Clarke[1,2], L Nhleko[1], A Charles[1,3], Z Phikiso[1] and T Dhansay[1]

[1]Council for Geoscience, Pretoria, South Africa
[2]Evolutionary Studies Institute, University of the Witwatersrand, Johannesburg, South Africa
[3]GEOSS South Africa (Pty) Ltd, Stellenbosch, South Africa

This study focused on the creation of a groundwater potential zones (GWPz) map for an area around the town of Franschhoek, Western Cape Province, South Africa. Parameters including lineament density, aquifer type data, distance to rivers, slope, land use land cover and rainfall were integrated using the geographic information system multi-criteria decision making (GIS-MCDM) weighted overlay method to create the map. Lineaments were obtained from existing geology maps and remote sensing datasets including ArcGIS basemaps, Satellite Pour l'Observation de la Terre (SPOT) 6, Landsat 8, Sentinel-2, Advanced Land Observing Satellite Phased Array type L-band Synthetic Aperture Radar (ALOS PALSAR) and airborne hyperspectral data. On the GWPz map, high potential zones covered 21% of the area, medium potential zones 42%, low potential zones 27%, and 10% had very low potential. 74% of the boreholes were drilled in the medium and high potential zones. Seismic and stress data were integrated with the GWPz and lineaments and the results showed that areas with high groundwater potential at the intersection of northeast–southwest lineaments would be good exploration targets. Sensitivity analyses involved creating scenario maps based on various weighting options and evaluating the results using Kappa and Pearson correlation coefficients and area under the receiver operating characteristic (ROC) curve (AUC). The scenario maps showed moderate to high correlation (0.67 to 0.96) and Kappa coefficients (23% to 75%) indicated fair to substantial agreement amongst the maps. AUC values ranging from 46% to 66% showed that the models' abilities to distinguish between the classes ranged from poor to average. The results showed that although the map changes with variations in parameter weights and classification, the high groundwater potential zones are not significantly affected. The findings of the study will assist decision makers in identifying suitable exploration areas, enabling efficient planning, allocation and management of resources.

CORRESPONDENCE
C Musekiwa

EMAIL
cmusekiwa@geoscience.org.za

DATES
Received: 31 January 2024
Accepted: 18 October 2025

KEYWORDS
groundwater potential
remote sensing
multi-criteria decision analysis
sensitivity analysis

INTRODUCTION

Water demand in the Western Cape Province, South Africa, is expected to increase in the future due to population growth and climate change. Periodic drought spells have put a strain on existing surface water resources, resulting in the need for augmentation with groundwater (GreenCape, 2019). There is also a need for proper management to ensure sustainable supply and protect resources against pollution and aquifer depletion. Groundwater potential mapping provides an understanding of the distribution of resources and enables better decision-making in planning for exploration and development of initiatives to avoid overextraction (Patel et al., 2024; Thahn et al., 2022). Groundwater potential is the probability that subsurface water can be developed for an area, denoting the likelihood of finding and effectively using the resource (Diaz-Alcaide, 2019).

Groundwater availability is largely affected by geology, with the porosity and permeability controlling the retention or transmission of water. Groundwater is transmitted and/or stored between pore-spaces, faults, fractures, joints and lineaments (Lin et al., 2015; Salako Adebayo and Adepelumi Abraham, 2018). Lineaments represent zones of faulting and fracturing which result in increased secondary porosity and permeability (Ceccato et al., 2022). Mapping of these geological features can be facilitated using remote sensing (RS) data and geographical information system (GIS) software. Aerial imagery, multispectral and hyperspectral satellite imagery are used as bases from which geological features are manually digitised. These data and others that influence groundwater potential are integrated using GIS to create GWPz maps. RS and GIS are cost-effective techniques that have been applied in numerous studies (e.g. Adesola et al., 2023; Al-Djazouli et al., 2021; Allafta et al., 2020; Arunbose et al., 2021; Benjmel et al., 2020; Duguma and Duguma 2022; Kabeto et al., 2022; Kamaraj et al., 2023; Khan et al., 2022; Owolabi et al., 2020; Priya et al., 2022; Qadir et al., 2020; Tamesgen et al., 2023).

Approaches used to create GWPz maps include MCDM, analytic hierarchy process (AHP), frequency ratio (FR) models, evidence belief function (EBF), weights of evidence (WOE), and machine learning. MCDM is widely used and its variant AHP is the most popular (Thanh et al., 2022; Şener et al., 2018). The integration of GIS and MCDM is termed GIS-MCDM. In this study, the GIS-MCDM approach was utilised because of ease of use and fast production of results. It is applicable in data-scarce regions as the parameters used can be reduced and expert knowledge can be incorporated to fill in the gaps (Malczewski, 2005; Thanh et al., 2022). It does not need available, accurate data, i.e., borehole data, to train the model, unlike machine learning techniques. The parameters are classified and assigned weights according to their relevance to groundwater potential. Parameter values are multiplied by their weights and summed to create the GWPz map. In a simplistic approach, the weights are assigned

by experts with guidance from literature sources. In the AHP approach, various experts perform pairwise comparisons of the parameters and assign numerical values that rank their influence on potential. These values are integrated to produce the weights. AHP is a more appropriate and scientific way of assigning weights to parameters but has its shortfalls.

A challenge of AHP is inconsistencies arising from the subjective values assigned by the experts. Although the addition of more experts might remove the subjectivity it sometimes adds to more disagreement. There is also often a shortage of experts with adequate knowledge of the subject under study (Adesola et al., 2023). Lastly, the increase in parameters lead to more complex comparisons. In this study, the weights were assigned based on the authors' judgements and guidance from literature (Macharis et al., 2004).

In South Africa, there is a need for more studies on groundwater potential mapping that incorporate high-resolution RS data such as airborne hyperspectral data and more recent satellite datasets like the Sentinel 2 data, and radio detection and ranging (RADAR) data like ALOS PALSAR (Adesola et al., 2023; Zhu and Abdelkareem, 2021). Detailed structural geology and analysis of the relationship between groundwater potential, earthquake focal mechanisms and stress have not been adequately assessed. This study aims to address these gaps and create a GWPz for an area in Franschhoek, in the Western Cape Province of South Africa, using the GIS-MCDM weighted overlay method. The groundwater potential is analysed in relation to earthquake focal mechanisms and stress data. Borehole data were used to validate the GWPz and scenario analysis performed to assess the effects of different weighting options on the results.

STUDY AREA

The study area is shown in Fig. 1, along with the elevation, which ranges from 130 to 1980 mamsl. The area receives winter rainfall between the months of May and October, whereas the summer months are hot and dry. Precipitation is orographically influenced and includes periodic snowfalls in the high mountain ranges during the winter months from June to September. Annual rainfall in the mountainous areas can be more than 1 000 mm, leading to high groundwater recharge (Mukhawana et al., 2024).

Franschhoek faces water challenges, including pollution, inadequate sanitation and drainage. Like most towns in South Africa, it also faces drought linked to climate change, which can impact water availability. The population of the area is also increasing, putting more strain on the existing water resources. There is a need for effective water demand management initiatives. The Integrated Development Plan for Stellenbosch Municipality (2024), within which Franschhoek is located, details the need to address water shortages by investigating and providing groundwater as a potential water source, as well as the need for conservation of existing sources. GWPz maps provide an indication of areas that can be targeted for exploration and protected against depletion and pollution. This contributes towards developing sustainable groundwater use plans and management frameworks.

Geology

Geologically, the area is located at the structural interface between the western arm and the Ceres syntaxis of the Permo-Triassic Cape Fold Belt (CFB). The CFB is a fold and thrust belt of late Paleozoic age, which affected the sequence of sedimentary rock layers of the Cape Supergroup in the southwestern corner of South Africa. The CFB is composed of a north-northwest (NNW) trending western branch stretching from Stellenbosch to Vanrhynsdorp and a southern branch with an east–west (E–W) axial orientation from Swellendam to the Great Fish River (between 25°E and 27°8'E). The two arms of the CFB meet in the structural Ceres syntaxis in the centre with more complex folding and faulting. The Ceres syntaxis is a broad structural region of the CFB that extends from the northeast of Ceres and southwards to Cape Hangklip (the area between the orange lines on the map in Fig. 2) (Booth, 2011; De Beer, 1990; Hälbich, 1992; Newton, 1993; Newton et al., 2006). The Ceres syntaxis is typified by intermediate northeast-trending fold axes in addition to interference sheath folds, superimposed folds, curved to bent folds and complex faults that trend northeast–southwest (NE–SW) to northwest–southeast (NW–SE) as well as north-south (De Beer, 1995, 1999).

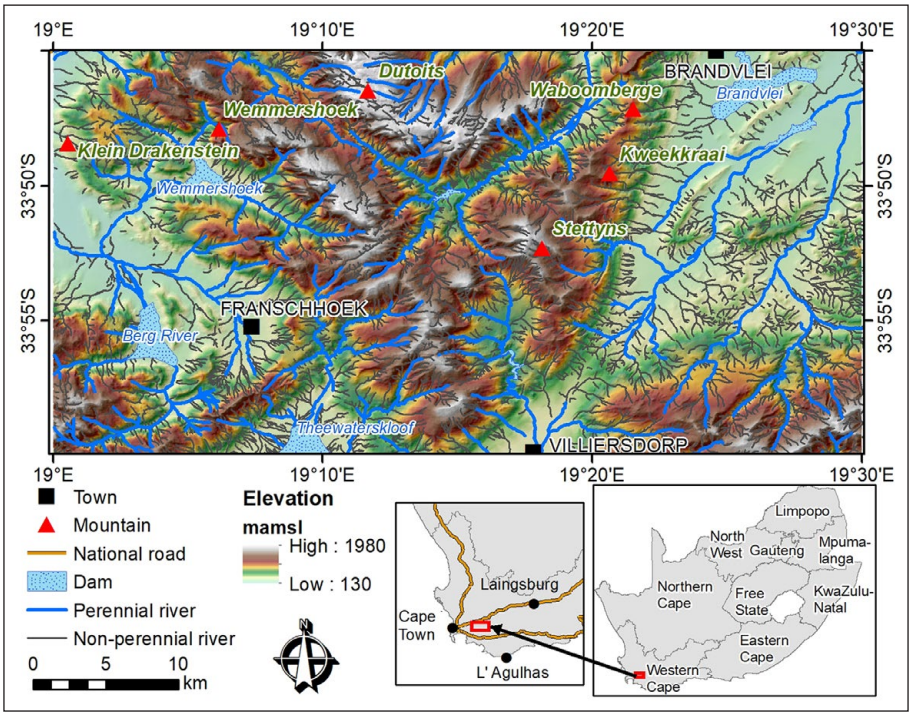

Figure 1. Map of the study area showing major rivers and elevation; insert maps at the bottom right show the location of the study area within South Africa

The CFB comprises rocks of the Malmesbury Group, Cape Granite Suite, Cape Supergroup as well as the Dwyka Group and lowermost Ecca Group. The Cape Supergroup is split into 3 groups: the Table Mountain, Bokkeveld, and Witteberg groups (Council for Geoscience, 2019). Quaternary-aged deposits are interpreted to be recent un- to semi-consolidated alluvial and collovial siliciclastics that have accumulated at the foot of valleys and are adjacent to rivers and streams (Fig. 2).

The major structural feature is the NE-trending 1st order Stettyns anticline (Fig. 2). The Stettyns anticline forms the mountains that dominate the Franschhoek area. Here the anticline manifests as a large 1st order fold in rocks of the predominantly arenaceous Table Mountain Group. The main 1st order axial plane of the Stettyns anticline forms on rocks of the more competent and arenaceous Peninsula Formation (part of the Table Mountain Group), with its major orientation inferred to run along the northeast-trending normal fault that separates the area's mountains.

Numerous faults and joints crosscut the lithostratigraphy and are conduits for recharge sites to the groundwater (Figs 3A–3C). These structural features form springs (eyes) in places where the perched groundwater intersects the topography of the landscape. The structural lineaments often act as sites for alteration, metasomatism (Fig. 3D) and precipitation of other minerals. The stockwork manganese oxide precipitates are shown in black in Fig. 3D. Manganese oxide is exclusively prevalent in stockworks of the Peninsula Formation and is attributed to supergene precipitation from the groundwater (De Villiers, 1960; Killick, 2020; Marchant et al., 1978; Theron et al., 1992). Although many of the structural lineaments in the area are open, others may be closed in places through welded fault gauges.

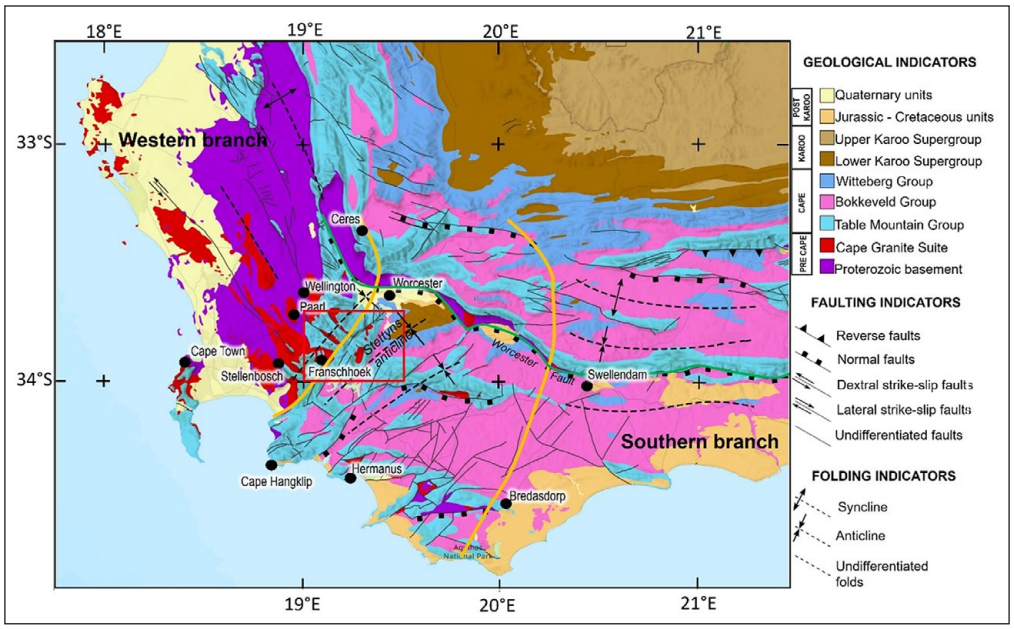

Figure 2. Structural features and domains associated with the Cape Fold Belt in the vicinity of the study area (the red polygon). The Ceres Syntaxis is approximated to be the area between the orange lines (Xu et al., 2009).

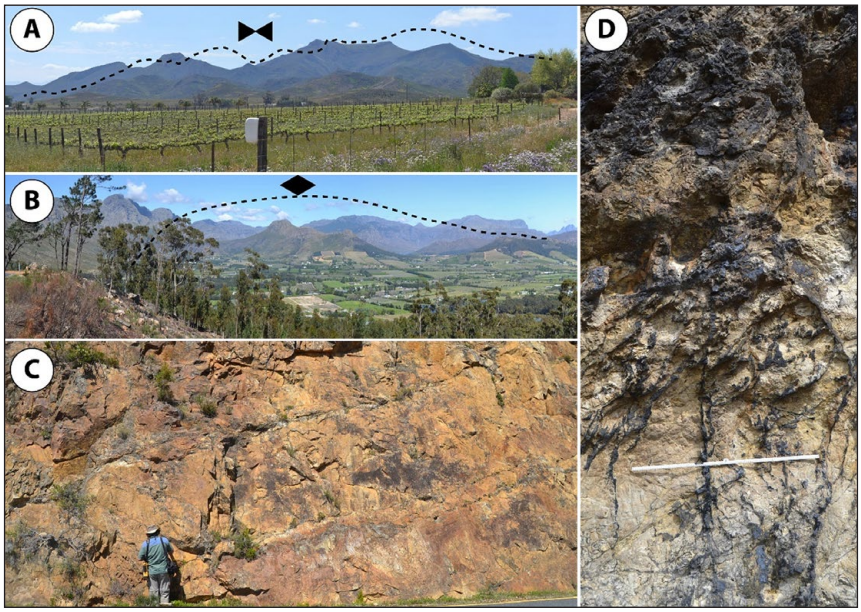

Figure 3. Major structural features in the study area. (A) Parasitic folding in rocks of the Bokkeveld Group in the Worcester syncline at Stettyns Mountain (dashed black line). (B) The Stettyns anticline at Franschhoek (dashed black line). (C) Fracturing in quartzites of the Peninsula Formation on Lambrechts Road to Franschhoek Pass, person for scale. (D) Stockwork manganese oxide precipitates in fractured quartzites of the Peninsula Formation at Franschhoek Pass, scale rule = 1.0 m.

METHODS

Data and processing

The methodology followed is presented in Fig. 4. Lineaments (which included faults) were manually digitised from multispectral RS and airborne hyperspectral data, geological maps and a hillshade derived from the 30 m spatial resolution Shuttle Radar Topography Mission (SRTM) elevation data (National Aeronautics and Space Administration Jet Propulsion Laboratory, 2013). Multispectral satellite imagery utilised included: Satellite Pour l'Observation de la Terre (SPOT) 6 (South African National Space Agency (SANSA, 2022)); Landsat 8 (Earth Resources Observation and Science (EROS) Center, 2020); Sentinel 2 (European Space Agency, 2019), ArcGIS base imagery; and ALOS PALSAR (Japan Aerospace Exploration Agency Earth Observation Research Center (JAXA EORC), 2025).

The airborne hyperspectral data used in this study were collected for the Council for Geoscience by SpecTIR Company during the year 2018.

Airborne hyperspectral imagery is the best dataset to utilise due to the high spatial and spectral resolution, but the cost of acquisition makes its use prohibitive. SPOT 6 and ArcGIS base imagery also have the high spatial resolution that is instrumental in highlighting lineaments. SPOT is not freely available; the data used in this study were obtained from South African National Space Agency (SANSA) through an agreement between SANSA and the Council for Geoscience. Table 1 shows the characteristics of the datasets shown in Fig. 5.

Processing techniques like band algebra, principal component analysis (PCA), minimum noise fraction transform (MNF) and directional filtering were applied to the RS imagery to highlight lineaments. The processing was done using PyGMI (Cole, 2024). Similar datasets and approaches have been used in other studies (e.g. Embaby et al., 2024; Ishola et al., 2023; Kabeto et al., 2022; Kamaraj et al., 2023; Morgan et al., 2022; Saravanan et al., 2021; Shebl et al., 2022; Smida et al., 2022; Upwanshi et al., 2023).

Digitised lineaments were verified using fieldwork and major directional trends were computed. Lineament density was calculated using the ArcGIS density tool and a cell size of 30 m was used to correspond to that of the SRTM data.

Aquifer types are grouped according to porosity and permeability. Higher porosity promotes groundwater storage and higher permeability contributes to increased water yields. Three aquifer types cover the area: intergranular, fractured and a combination of intergranular and fractured (Meyer, 2001) (Fig. 6). The fractured aquifer is the largest, covering 78% of the area. Boreholes drilled in this aquifer can yield more than 5 L/s. The intergranular aquifer is generally unconsolidated with occasional semi-consolidated units and is characterised by tertiary-quaternary coastal and alluvial deposits. The aquifer makes up approximately 20% of the area and boreholes in this aquifer can yield up to 2 L/s.

The fractured and intergranular aquifer is characterised by medium- to coarse-grained granite weathered to varying thicknesses. It occupies 2% of the area and the borehole yields in this aquifer can go up to 0.5 L/s (Meyer, 2001). The aquifer type data were obtained from the South African national Department of Water and Sanitation in vector format and converted to raster at 30 m spatial resolution (Fig. 6).

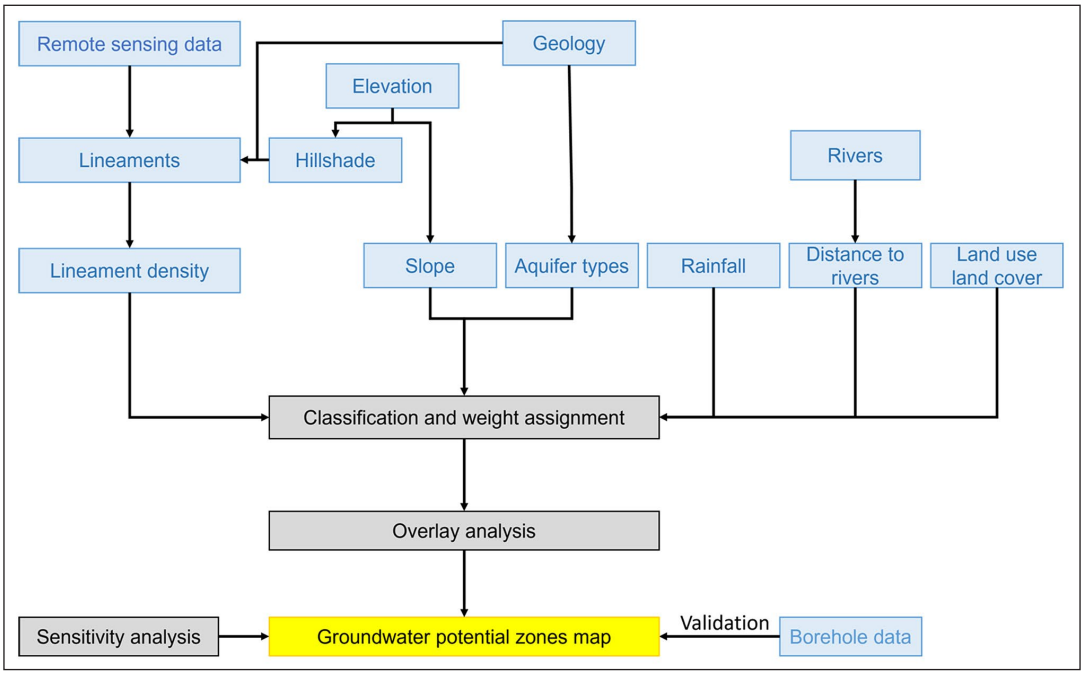

Figure 4. Methodology of the study (blue rectangles represent datasets; grey rectangles represent processes)

Table 1. RS datasets used (IR = infrared, SWIR = shortwave infrared, TIR = thermal infrared)

Dataset	Spatial resolution (band)	Number of bands	Acquisition date
SPOT 6	1.5 m (panchromatic); 6 m (blue, red, green, near IR)	4	April 2015
Landsat 8	15 m (panchromatic); 30 m (visible, near IR, SWIR); 100 m (thermal band)	11	December 2013
Sentinel 2	10 m; 20 m; 60 m (visible, near IR, SWIR)	12	March 2017
Airborne hyperspectral	3 m (VNIR, SWIR)	322	August and September 2018

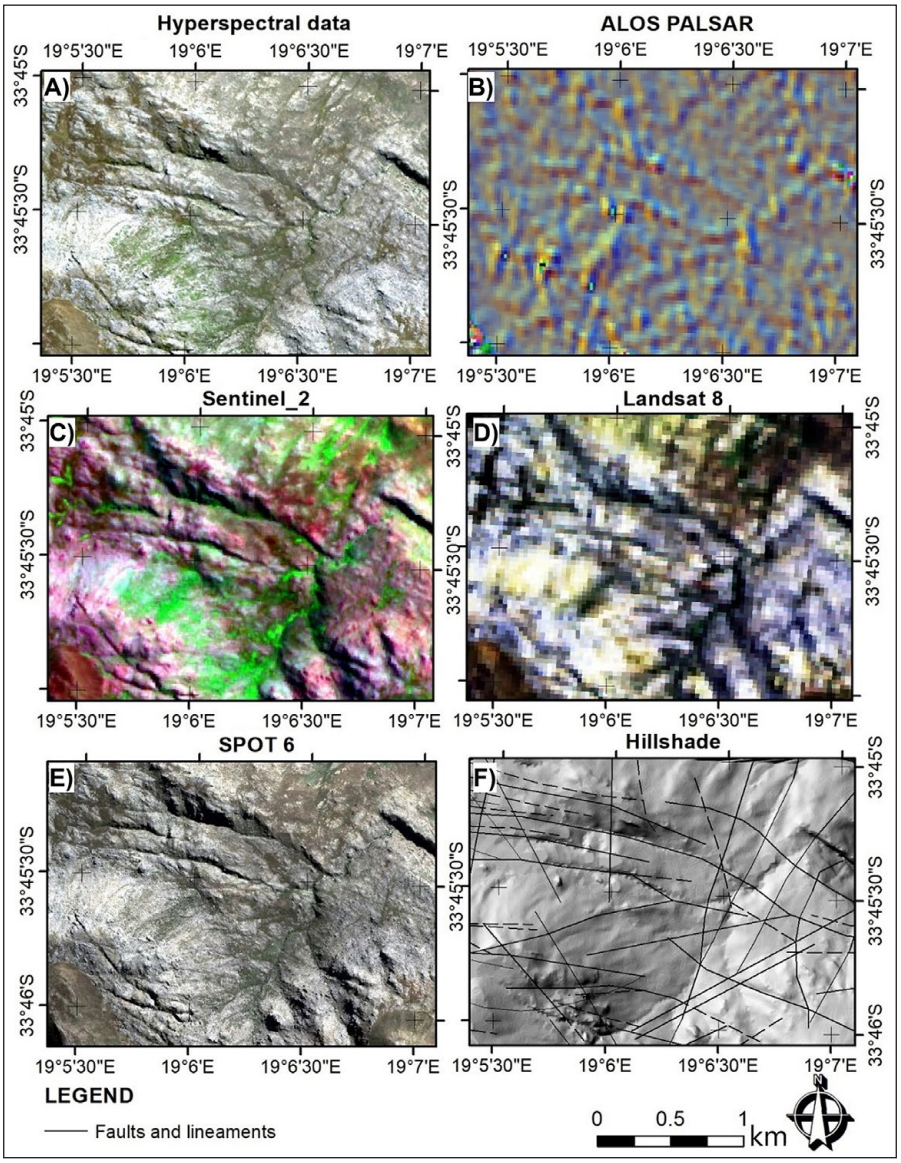

Figure 5. Remote sensing imagery: (A) airborne hyperspectral data (red = Band 39, green = Band 64, blue = Band 194); (B) filtered ALOS PALSAR; (C) Sentinel 2 (red = Band 12, green = Band 8, blue = Band 3); (D) Landsat 8 (red = Band 4, green = Band 3 and blue = Band 1); (E) SPOT 6, and (F) SRTM hillshade and lineaments

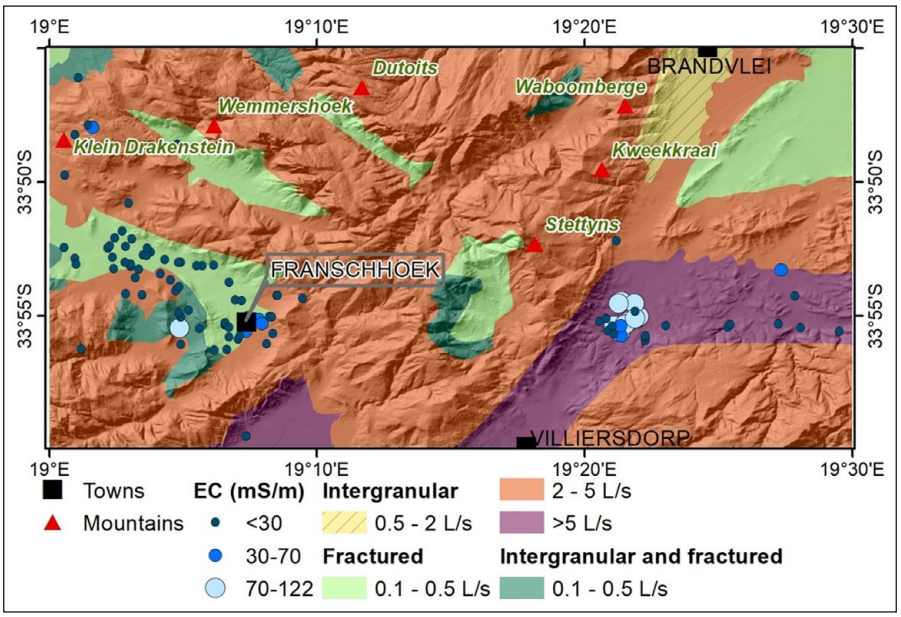

Figure 6. Aquifer types with borehole yields shown in litres per second (L/s) and borehole data symbolised according to electrical conductivity (EC) in millSiemens per meter (mS/m).

High intensity and short duration rainfall causes less infiltration and more surface runoff, while low intensity and long duration rain results in higher infiltration and less run-off (Arulbalaji et al., 2019; Abdalla et al., 2020). High rainfall indicates an increase in recharge and higher groundwater potential, whereas low rainfall leads to lower recharge. Mean annual precipitation data were obtained from the Agricultural Research Council Institute for Soil Climate and Water (ARC–ISCW, 2004) (Fig. 7).

Slope indicates the steepness or incline of a surface and influences surface runoff, ponding and the rate of infiltration of surface water into the aquifer. Slope was derived from the SRTM data. Areas with lower slope values have a lower hydraulic gradient, thus enhanced runoff infiltration and recharge of aquifers (Abdalla et al., 2020; Arulbalaji et al., 2019). The flat slopes have the highest groundwater potential (Fig. 7). Slope was derived from the SRTM elevation dataset.

Rivers can recharge groundwater, implying that areas on or close to rivers have higher groundwater potential. The 1:50 000 scale river lines were obtained from the Department of Rural Development and Land Reform: National Geo-spatial Information Division (DRDLR, 2022). Buffers were created along the rivers and subdivided into 3 classes representing low, medium, and high categories. In close proximity to the river there is high groundwater potential as there is a higher likelihood of intercepting groundwater during drilling. The buffer vector file was converted to raster at a 30 m spatial resolution (Fig. 7).

Land use and land cover can alter recharge rates, by either reducing or increasing them. In this study, water bodies and forests are assumed to have high groundwater potential as they increase infiltration and recharge, while built up areas and barren land are assigned low groundwater potential as they limit infiltration. This is a simplified assumption, applicable to regional-scale studies, whereas in some cases deep-rooted plants can also limit recharge as they extract water from the aquifer. In more localised studies, the complex relationship between land use land cover and recharge must be studied in detail. The land use data were sourced from the South African National Land Cover Data (SANLC) (DEA, 2018) in raster format at a spatial resolution of 20 m. Similar classes were grouped together (Fig. 7).

Creation of the GWPz map

Each parameter layer was classified into ranges and values were assigned depending on their groundwater potential as follows: 3 = high potential, 2 = medium potential and 1 = low potential. The slope was classified according to the standard SOTER (Soil and TERrain) classification (Van Engelen and Dijkshoorn, 2012). The distance to river was classified according to authors' judgements guided by literature. Lineament density was classified according to quantiles and rainfall by the Jenks natural breaks classification. This is the most widely used method as it identifies natural groups inherent in data. It aims to reduce variances within classes and maximise differences between classes (Brewer and Pickle, 2003). The parameters (Fig. 7) were assigned weights indicating their

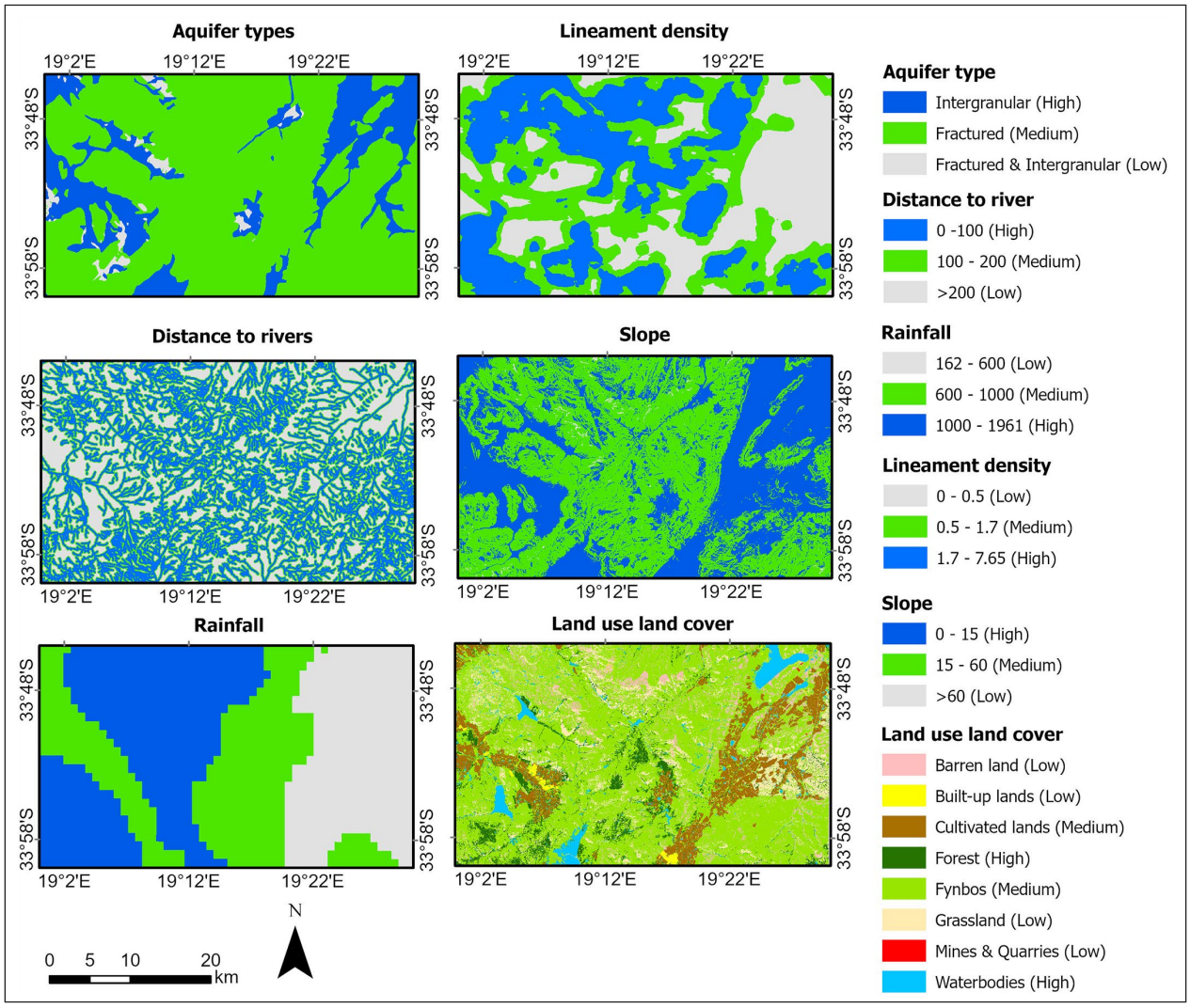

Figure 7. Datasets used in creating the GWPz map

Table 2. Parameter classes and weights

Parameter	Weight	Class	Groundwater potential	Value	% area
Distance to rivers (metres)	0.1	0–100	High	3	31.42
		100–200	Medium	2	25.36
		> 200	Low	1	43.21
Aquifer types	0.25	Intergranular	High	3	20.39
		Fractured	Medium	2	77.51
		Intergranular & fractured	Low	1	2.10
Lineament density (kilometres/square kilometres)	0.2	1.7–7.6	High	3	43.21
		0.5–1.7	Medium	2	25.36
		0–0.5	Low	1	31.42
Slope (degrees)	0.2	0–15	High	3	41.36
		15–60	Medium	2	55.0
		> 60	Low	1	3.64
Rainfall (millimetres/year)	0.15	1 000–1 961	High	3	0.36
		600–1 000	Medium	2	0.29
		162–600	Low	1	0.35
Land use land cover	0.1	Barren land	Low	1	5.03
		Built-up lands	Low	1	0.93
		Cultivated lands	Medium	2	10.44
		Forest	High	3	6.43
		Fynbos	Medium	2	63.45
		Grasslands	Low	1	9.61
		Mines and quarries	Low	1	0.02
		Waterbodies	High	3	4.09

Table 3. Scenarios and the parameter weights

Parameter	Scenarios							
	Base	2	3	4	5	6	7	8
Distance to rivers	0.1	***0.3***	0.1	0.1	***0.2***	***0.15***	0.1	0.1
Aquifer types	0.25	***0.2***	***0.1***	***0.15***	***0.1***	***0.2***	0.25	0.25
Lineament density	0.2	***0.1***	***0.3***	***0.15***	0.2	***0.1***	0.2	0.2
Slope	0.2	0.2	***0.15***	***0.3***	***0.1***	***0.15***	0.2	0.2
Mean annual rainfall	0.15	***0.1***	***0.2***	0.15	***0.3***	***0.1***	0.15	0.15
Land use land cover	0.1	***0.2***	***0.15***	***0.15***	0.1	***0.3***	0.1	0.1

Weights that changed from the base scenario are highlighted in bold italics

relative importance to groundwater potential based on authors' expert knowledge and findings from other similar studies (Table 2). The lineament density, aquifer types, slope, rainfall, distance to rivers and land use landcover parameters were combined using the GIS-MCDM weighted overlay method in ArcGIS Pro 3.3.0 to produce the GWPz map.

Some of the shortfalls of the GIS-MCDM weighted overlay approaches include the use of arbitrary classifications and subjective weighting methods. There is a need to provide metrics for the evaluation of the effects of variations of classifications and weights on the output. The model outputs can be affected by: (i) the number of input parameters; (ii) inaccuracies related to inputs, weights, and ranks assigned; and (iii) the nature of the method used to integrate the data. Sensitivity analyses are recommended to assess the robustness of the model outputs due to variations in input variables and parameter weights (Hagenlocher et al., 2019; Thapa et al., 2018).

Sensitivity analyses were performed by creating scenario maps based on different parameter weightings and classification methods. Seven scenarios were tested, five included the variations of the parameter weights only and two included parameter weights and different classification methods for lineament density and mean annual rainfall. The weighting options for the different scenario maps are shown in Table 3. The weights were assigned based on expert knowledge and findings from literature. The weights that changed from the base scenario are highlighted in bold italics.

Scenarios 7 and 8 included classifications for rainfall based on quantiles and lineament density based on Jenks natural breaks (Table 4). Quantile classification divides the data into classes ensuring that each class has the same number of data values (GISGeography, 2015). This classification method has been used in similar studies (e.g. Adesola et al., 2023; Lee et al., 2019; Thamaga et al., 2024).

Table 4. Quantile classification of lineament density and rainfall

Parameter	Class	Groundwater occurrence potential
Lineament density	2.9–7.6	High
	0.1–2.9	Medium
	0–0.1	Low
Mean annual rainfall	1 347–1 961	High
	748–1 347	Medium
	162–748	Low

The results were assessed using Pearson correlation and Kappa coefficients. Correlation coefficients show the strength and direction of relationship between two maps, with values from 0.70 to 1.00 showing high correlation. The Kappa comparison compares two maps at a time, cell-by-cell, to determine if they are in spatial agreement. Kappa coefficients from 0.40 to 1.00 show moderate to almost perfect agreement. Kappa coefficients were calculated using the Map Comparison Kit (Research Institute for Knowledge Systems (RIKS BV), 2010; Hagen, 2002).

The scenario maps were validated using borehole data and area under the receiver operating characteristic (ROC) curve (AUC) (Thamaga et al., 2024). This is the most utilised technique to evaluate the performance of the models' abilities to discriminate between different groundwater potential classes (Thanh et al., 2022). AUC values were computed using the ArcSDM add-on to ArcGIS software. There are 5 categories of AUC: (1) poor (0.5–0.6); (2) average (0.6–0.7); (3) good (0.7–0.8); (4) very good (0.8–0.9); and (5) excellent (0.9–1) (Çorbacıoğlu et al., 2023; Dar et al., 2020).

RESULTS

Lineament analyses

Pearson correlation was conducted between the borehole water levels and the lineament density and a very weak negative correlation of −0.06 was found. This result is similar to findings from other studies (e.g. Tessema et al., 2011; Embaby et al., 2023; Shaban et al., 2007). This can be attributed to some of the following reasons: uncertainties in mapping of lineament (not all maps are visible and can be mapped); the density map is scale dependent and might not the representative of the area (Jia and Lin, 2010); too few boreholes to do the statistical analysis; poor spatial accuracy of input borehole data; and borehole water levels are also affected by other factors including geology and aquifer characteristics (Bon et al., 2022).

Figure 8 shows the distribution of the lineament orientations. Figure 9 displays the orientations and fold azimuths which trend north-east, and the major mode of linear features are oriented east–west (E–W) followed by southwest–northeast (SW–NE).

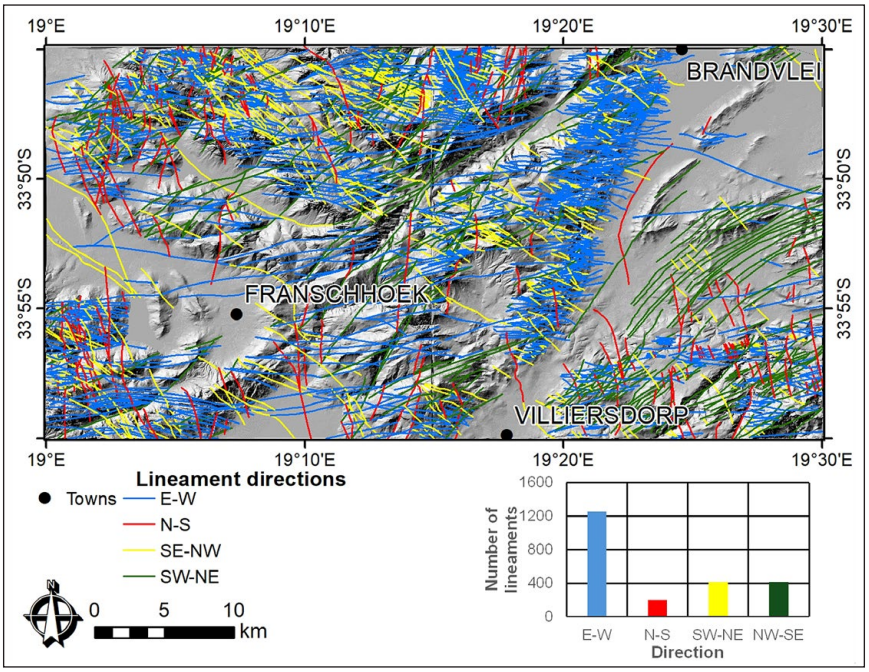

Figure 8. Lineaments classified in four main orientations

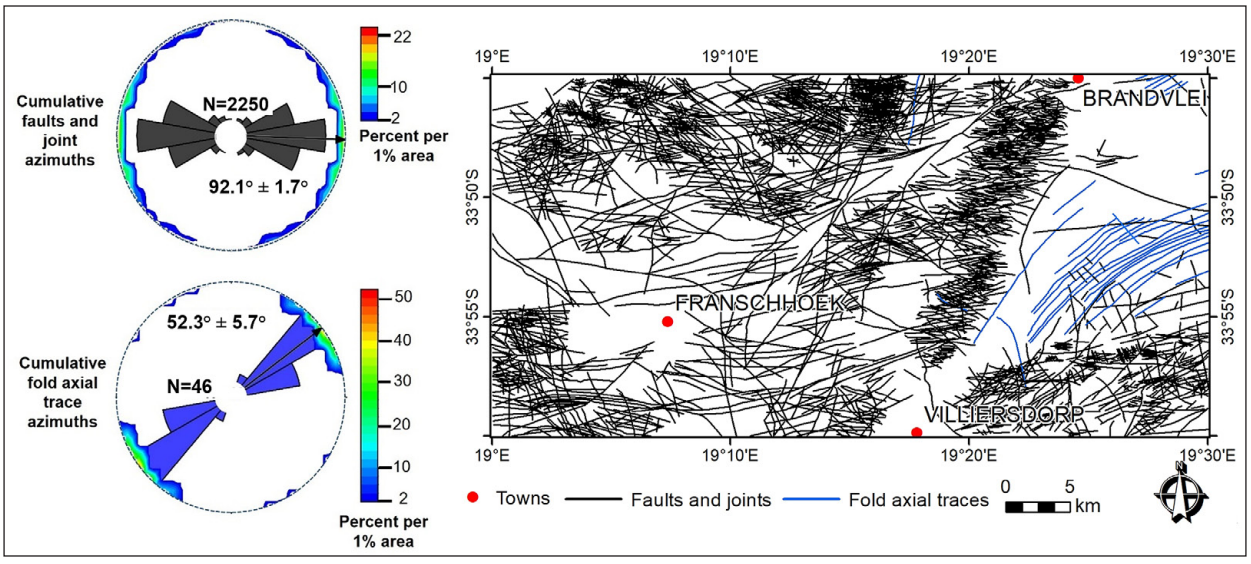

Figure 9. Rose diagrams of the lineaments grouped into two classes: faults and joints and fold axial traces

The aperture range and degree of interconnection controls the availability of water and the speed with which it flows. The dominant E–W trend and two joint systems were observed: System 1 = E–W and southwest–northeast (SW–NE) / southeast–northwest (SE–NW) and System 2 = north–south (N–S).

The interplay between the mapped lineaments and the surrounding stress fields plays an important role in the movement and concentration of groundwater (Dhansay, 2021). Earthquake focal mechanisms (Manzunzu et al., 2019) and data from the World Stress Map (Heidbach et al., 2018) suggest that the maximum horizontal stress across the study area is extensive and oriented approximately E–W with a predominance of normal and strike-slip faulting (Fig. 10). The orientation of mapped lineaments and the surrounding stress fields suggest that the mapped approximately NE–SW oriented lineaments may act as normal faults, while the E–W oriented lineaments may act as strike-slip faults. This would imply that within the study area, lineaments that are oriented NE–SW would hold the highest groundwater potential. This is because this orientation of fractures, relative to the surrounding stress field, would enable the highest permeability pathways.

Groundwater potential zones map

The GWPz map was classified into 4 categories using the natural breaks classification: (very low: 1.20–1.84; low: 1.85–2.09; medium: 2.10–2.35; high: 2.36–3) (Fig. 11). Natural breaks classification was

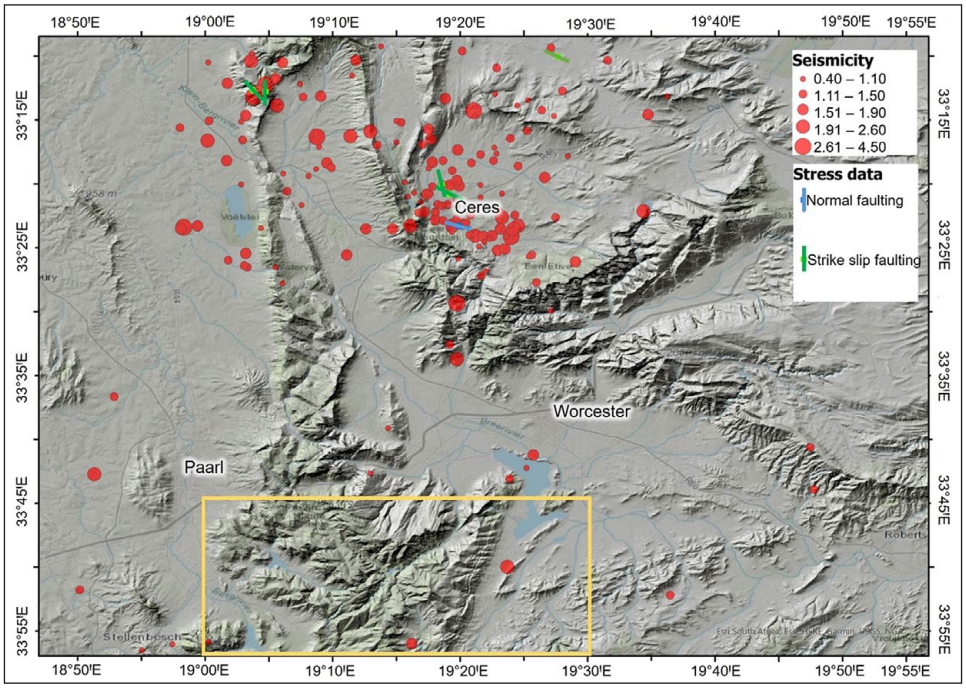

Figure 10. Maximum horizontal stress indicators and seismicity information surrounding the study area (shown in orange)

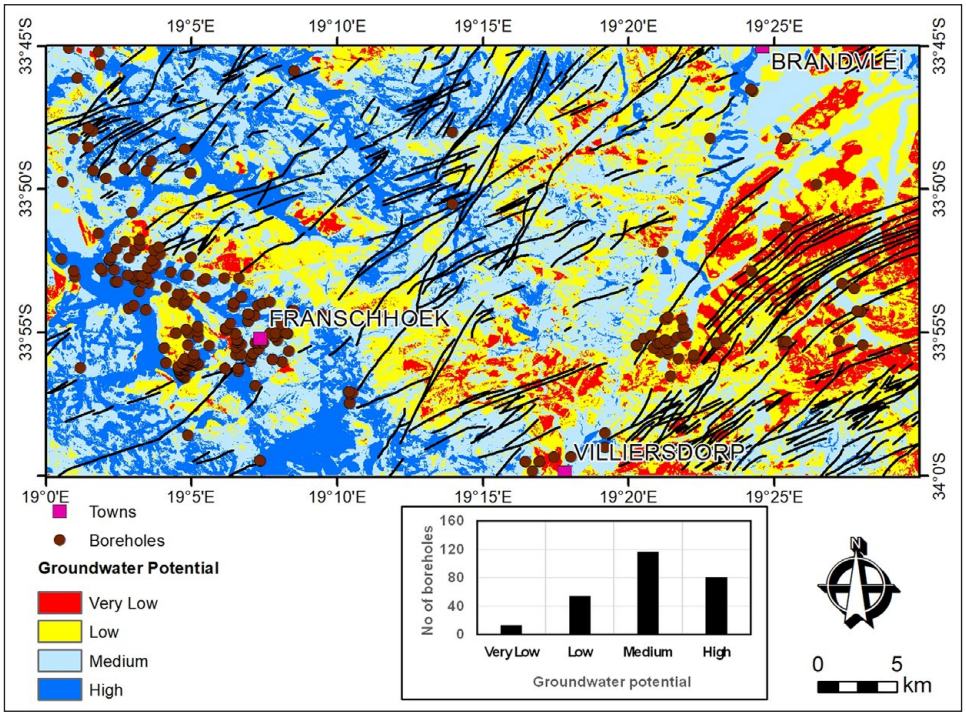

Figure 11. GWPz map showing the groundwater potential classes; NE–SW lineaments shown in black and a graph showing the boreholes per class

used in similar studies found in the literature (Thapa et al., 2018; Guru et al., 2017). Four classes were selected to show more variation on the map as opposed to the three used in the input data; the classes do not necessarily need to be the same (Rana et al., 2025; Shandu and Atif, 2023; Zhu and Abdelkareem, 2021). High groundwater potential covers about 21% of the area; medium potential zones occupy 45%; 27% of the area is in the low potential zones; and 10% of the area has very low groundwater potential. Out of a total of 266 boreholes, 44% were drilled in medium groundwater potential zones, 30% are in the high groundwater potential areas, 21% in low potential zones and 5% in very low potential zones.

Areas of high potential that intersect NE–SW trending lineaments would be ideal areas for exploration (Fig. 11). Visual interpretation of the results show that some boreholes were drilled in these target areas. Statistical analyses cannot be conducted and would provide inaccurate results due to the inaccuracies arising from borehole location and the surface expression of the lineaments. Lineaments often cannot be accurately mapped in some areas due to interpretation subjectivity, quality of the data used, coverage by vegetation or other surface phenomena. The mapped lineaments are simply represented by a line but can be wider, longer and be dipping at depth (Adam et al., 2025). Figure 12 shows the water levels of the boreholes per groundwater potential class.

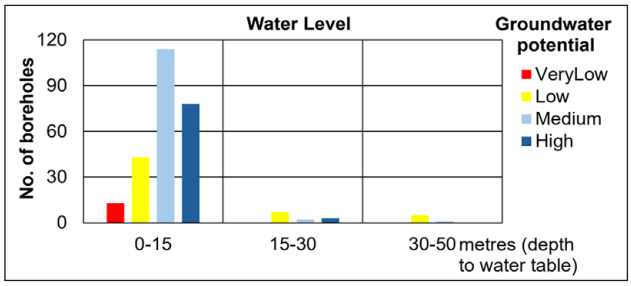

Figure 12. Number of boreholes in each water level class per groundwater potential

Sensitivity analyses

Correlation analysis between the GWPz maps created from various scenarios shows moderate to high correlation; values obtained ranged from 0.67 to 0.96 (Schober et al., 2018) (Table 5). The Scenario 2 map is the least correlated to other maps because the weighting option varies the most (Fig. 13).

Table 5. Correlation analysis of the scenario maps; the low values are in bold italics

Scenario	1	2	3	4	5	6	7	8
1	1.00							
2	***0.78***	1.00						
3	0.91	***0.67***	1.00					
4	0.96	***0.79***	0.83	1.00				
5	0.86	***0.77***	0.94	***0.79***	1.00			
6	0.96	0.90	0.91	0.94	0.93	1.00		
7	0.96	***0.77***	0.83	0.94	***0.77***	0.91	1.00	
8	0.93	***0.76***	0.80	0.92	***0.79***	0.90	0.90	1.00

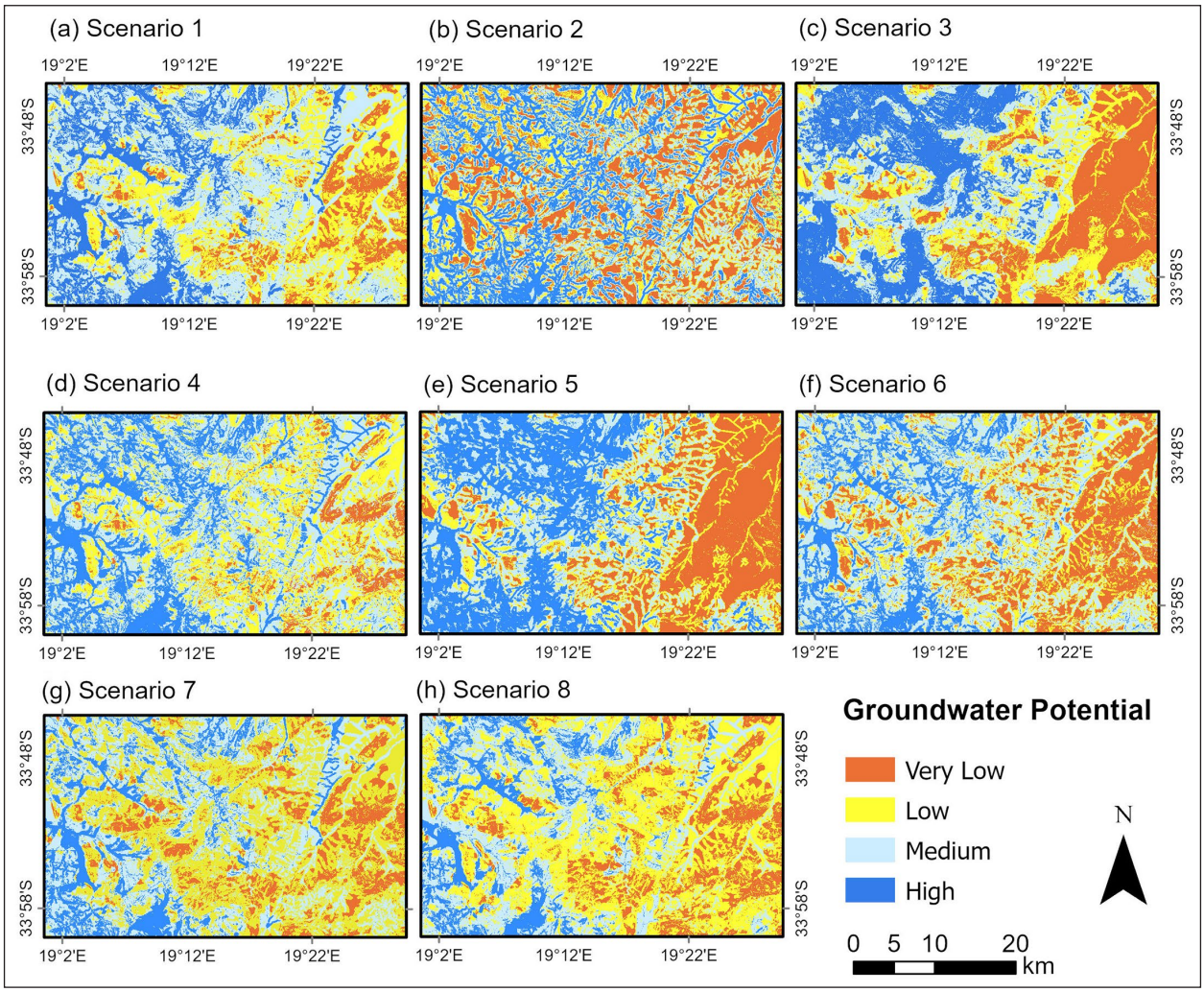

Figure 13. GWPz maps for all scenarios

Kappa coefficients indicate that there is fair to substantial agreement amongst the maps. The maps with the lowest Kappa coefficients are indicated in bold italics (Table 6). The Scenario 2 map is the most dissimilar to other maps because the 'distance to river' parameter has been weighted higher than in other scenarios.

The graph in Fig. 14 shows the proportion of cells per scenario for each groundwater potential zone. The results show that the 'low' category has the most substantial sensitivity (greater than 20% area change) between Scenarios 5 and 8 (Latunde and Bamigbola, 2018). The 'medium' and 'high' classes have the lowest changes, from 15–17%.

The graph in Fig. 15 shows the number of boreholes per scenario for each groundwater potential zone. This analysis is similar to that conducted for other studies (e.g. Guduru and Jilo, 2022; Berhanu and Hatiye, 2020). For most scenarios the majority of the boreholes are in the 'medium' and 'high' potential classes (ranging from 54–84%). The exception is Scenario 3 (46%) in which slope and aquifer types were assigned lower weights.

For validation of the GWPz scenario map, borehole data were used, and AUC values were calculated based on the location of 266 boreholes. The AUC values for the scenarios were: Scenario 1 (64%); Scenario 2 (59%); Scenario 3 (48%); Scenario 4 (67%); Scenario 5 (52%); Scenario 6 (60%), Scenario 7 (65%) and Scenario 8 (66%). The overall results show poor to average model predictive accuracy.

DISCUSSION

This research focused on the creation of a GWPZ map and contributes to the body of knowledge generated by other researchers in South Africa (e.g. Shandu and Atif, 2023; Adesola et al., 2023). Lineament density, aquifer types, rivers, slope, rainfall and land use land cover were integrated to create a GWPz map using the GIS-MCDM weighted overlay method. Lineaments were derived from RS data. The main challenge in the application of RS was the high vegetation cover in the area, which conceals geological features. The low resolution of some of the datasets and noise in others, for example RADAR, affects the usefulness of RS.

Table 6. Kappa coefficients with low values shown in bold italics

Scenario	1	2	3	4	5	6	7	8
1	1.00							
2	***0.32***	1.00						
3	0.46	***0.27***	1.00					
4	0.75	***0.38***	***0.33***	1.00				
5	***0.37***	***0.35***	0.61	***0.34***	1.00			
6	0.63	0.47	0.49	0.57	0.54	1.00		
7	0.62	***0.26***	***0.26***	0.47	***0.23***	0.53	1.00	
8	0.52	***0.24***	***0.24***	***0.38***	***0.25***	0.49	0.60	1.00

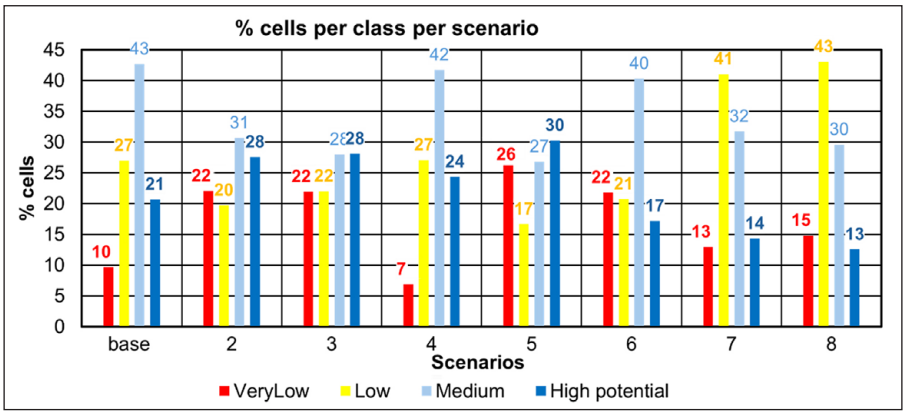

Figure 14. Proportion of cells for each groundwater potential class for the eight scenarios

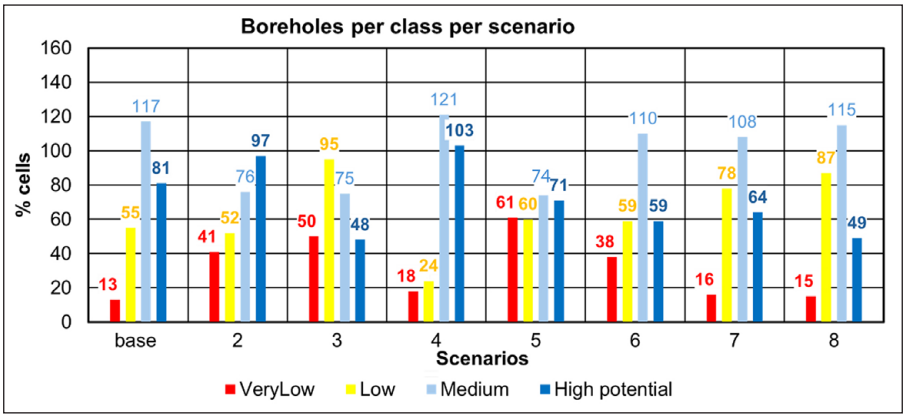

Figure 15. Number of boreholes for each groundwater potential class for the eight scenarios

A recommendation from this study is the use of various RS datasets, as they complement each other and highlight different aspects of the geology, as also highlighted by Zhu and Abdelkareem (2021) for a similar study. Fieldwork is often required to verify the results.

The GWPz map was classified into 4 classes using the natural breaks classifications. These ranged from very low to low, medium and high. The results showed that 74% of the boreholes were drilled in medium to high potential areas. The high groundwater potential areas are linked to low slope, the fractured Table Mountain Group aquifer and the medium areas to high lineament density. Lineament analysis and the study of seismicity and stress fields indicate that areas of high potential that intersect NE–SW trending lineaments would be ideal areas for groundwater exploration.

The GWPz map was validated using the ROC (AUC) approach and a value of 0.64 was obtained, implying that the model's ability to map GWPz classes was average. Sensitivity analyses were conducted to test the effects on the results of assigning varying weights and classes. Seven scenario maps were investigated and the differences assessed using correlation and Kappa coefficients. The scenario maps showed moderate to high correlation, with correlation values ranging from 0.67–0.96. The Kappa coefficient showed that the scenario maps have fair and substantial agreement. Although the weighting of the parameters affects the map, the high groundwater potential areas are not significantly affected. The maps were validated using borehole data and the AUC values ranged from 46% to 66%. This showed that the models perform poorly in distinguishing between the different classes. The results can be attributed to various factors, including incomplete and inaccurate validation data, use of low-resolution datasets (e.g., rainfall), incorrect weighting of parameters and non-inclusion of other factors that affect potential (e.g., the nature of the aquifer and groundwater levels). Inaccurate assignment of weights will produce a map that incorrectly represents potential and will be less reliable in exploration. These limitations have been highlighted in similar studies (e.g. Adesola et al., 2023; Adesola et al., 2025; Al-Abadi et al., 2023; Shandu and Atif, 2023).

CONCLUSIONS

This study offers a simple and methodical way to create maps of groundwater potential zones (GWPz) . The validation was conducted using the location of boreholes and ROC (AUC) metrics. Average AUC values obtained are similar to those from other studies (e.g. Gulbet Tebege et al., 2025). Ideally groundwater monitoring data, which are a true representation of the resource, should be used in validation of the result. Monitoring of groundwater levels and hydrochemistry data could not be used as these were not available at the time of the project's execution.

The discretisation of the data into classes for modelling and analysis processes introduces errors. The choice of a different classification method will yield different results and statistics. Discretisation is inevitable as some of the validation metrics cannot handle continuous data. In more detailed studies, various classification regimes can be tested and through sensitivity analyses (as shown in this study), an appropriate selection can be made. The results can then be verified using monitoring data.

The datasets and methodologies used in this study can be applied to any region and scale, although some of the datasets used in this study are too generalised to utilise for local-scale applications. In such studies, in-depth analysis of factors affecting groundwater occurrence is required (Adesola et al., 2023). The methodology is beneficial for research in data-scarce areas as parameters with unavailable data can be omitted from the model. The model will still produce results with limited datasets.

The farming community would benefit from the GWPz map as it provides an indication of the available groundwater resources. At a local scale, more detailed analysis of the borehole characteristics is required before borehole siting. GWPz areas defined on the maps can be conserved against severe depletion and pollution, thus contributing towards developing sustainable groundwater use and management frameworks.

CONFLICT OF INTEREST

There was no conflict of interest for any party involved in this research work.

ACKNOWLEDGMENTS

The authors would like to thank the Council for Geoscience for providing the data and for their financial support.

AUTHOR CONTRIBUTIONS

Chiedza Musekiwa – manuscript preparation, remote sensing, groundwater potential modelling; Lebogang Nhleko – geohydrology, groundwater potential conceptual model and manuscript preparation; Albie Charles – groundwater potential modelling, manuscript preparation; Zininzi Phikiso – groundwater potential modelling, manuscript preparation; Cameron Penn Clarke – geology, lineament analysis and manuscript preparation; Taufeeq Dhansay – geology, stress and seismic analysis, manuscript preparation.

ORCIDS

Chiedza Musekiwa
https://orcid.org/0000-0003-4865-3521

Cameron Penn-Clarke
https://orcid.org/0000-0003-2054-4673

Lebogang Nhleko
https://orcid.org/0000-0001-9298-4833

Zininzi Phikiso
https://orcid.org/0000-0003-4718-783X

Taufeeq Dhansay
https://orcid.org/0000-0001-9742-3998

REFERENCES

ABDALLA F, MOUBARK K and ABDELKAREEM M (2020) Groundwater potential mapping using GIS, linear weighted combination techniques and geochemical processes identification, west of the Qena area, Upper Egypt. *J. Taibah Univ. Sci.* **14** (1) 1350–1362. https://doi.org/10.1080/16583655.2020.1822646

ADAM RN, SCOTT C, ARROWSMITH JR, REANO D, MADUGO C, KOEHLER RD, ZUCKERMAN MG, GRAY B, KOZACI O, GONZÁLEZ T, ABRAMSONWARD H, ROCKWELL TK, GATH E, KOTTKE AR and LEUCHTER E (2025) A systematic approach to mapping tectonic faults and documenting supporting geomorphology. *Geosphere* **21** (2) 227–244. https://doi.org/10.1130/GES02767.1

ADESOLA G, THAMAGA KH, GWAVAVA O and PHAROE BK (2023) Groundwater potential zones assessment using geospatial models in semi-arid areas of South Africa. *Land* **12** (10) 1–20. https://doi.org/10.3390/land12101877

ADESOLA GO, GWAVAVA O, PHAROE BK, BAIYEGUNHI C, THAMAGA KH and MUAVHI N (2025) Appraising the accuracy of GIS-based bivariate statistical model for groundwater potential mapping in South Africa. *Heliyon* **11** (10) https://doi.org/10.1016/j.heliyon.2025.e43411

ARC – ISCW (Agricultural Research Council – Institute For Soil, Climate, And Water, South Africa) (2004) Overview of the status of the agricultural natural resources of South Africa – mean annual precipitation spatial data. ARC-ISCW Report No. GW/A/2004/13. ARC-ISCW, Pretoria.

AL-ABADI AM, JABBAR FK and HANDHAL AM (2023) Limitations of GIS-based groundwater potential mapping. *Arab. J. Geosci.* **16** (307). https://doi.org/10.1007/s12517-023-11405-1

AL-DJAZOULI MO, ELMORABITI K, RAHIMI A, AMELLAH O and FADIL OAM (2021) Delineating of groundwater potential zones based on remote sensing, GIS and analytical hierarchical process: a case of Waddai, eastern Chad. *GeoJournal*, **86** 1881–1894. https://doi.org/10.1007/s10708-020-10160-0

ALLAFTA H, OPP C and PATRA S (2020) Identification of groundwater potential zones using remote sensing and GIS techniques: a case study of the Shatt Al-Arab Basin. *Remote Sens.* **13** (1) 1–18. https://doi.org/10.3390/rs13010112

ARULBALAJI P, PADMALAL D and SREELASH K (2019) GIS and AHP techniques based delineation of groundwater potential zones: a case study from Southern Western Ghats, India. *Sci. Rep.* **9** (2082) 1–17. https://doi.org/10.1038/s41598-019-38567-x

ARUNBOSE S, SRINIVAS Y, RAJKUMAR S, NAIR NC and KALIRAJ S (2021) Remote sensing, GIS and AHP techniques-based investigation of groundwater potential zones in the Karumeniyar river basin, Tamil Nadu, southern India. *Groundwater Sustain. Dev.* **14** 1–13. https://doi.org/10.1016/j.gsd.2021.100586

BENJMEL K, AMRAOUI F, BOUTALEB S, OUCHCHEN M, TAHIRI A and TOUAB A (2020) Mapping of groundwater potential zones in crystalline terrain using remote sensing, GIS techniques, and multicriteria data analysis (Case of the Ighrem Region, Western Anti-Atlas, Morocco). *Water* **12** (2) 1–16. https://doi.org/10.3390/w12020471

BERHANU KG and HATIYE SD (2020) Identification of groundwater potential zones using proxy data: case study of Megech Watershed, Ethiopia. *J. Hydrol. Region. Stud.* **28** 100676. https://doi.org/10.1016/j.ejrh.2020.100676

BOOTH PWK (2011) Stratigraphic, structural and tectonic enigmas associated with the Cape Fold Belt: challenges for future research. *S. Afr. J. Geol.* **114** (3–4) 235–248. https://doi.org/10.2113/gssajg.114.3-4.235

BON AF, OMBOLO A, BIBOUM PM, MOUTLEN JM and MBOUDOU GE (2022) Identification of hydrogeological features using remote sensing and electromagnetic methods in the hard-rock formations of the Cameroon coastal plain (Central Africa): implications for water borehole location. *Sci. Afr.* **17** e01272. https://doi.org/10.1016/j.sciaf.2022.e01272

BREWER CA and PICKLE L (2003) Evaluation of methods for classifying epidemiological data on choropleth maps in series. *Ann. Assoc. Am. Geogr.* **92** (4) 662–681. https://doi.org/10.1111/1467-8306.00310

CECCATO A, TARTAGLIA G, ANTONELLINI M and VIOLA G (2022) Multiscale lineament analysis and permeability heterogeneity of fractured crystalline basement blocks. *Solid Earth* **13** (9) 1431–1453. https://doi.org/10.5194/se-13-1431-2022

DRDLR (Department of Rural Development and Land Reform, South Africa (2022) Electronic dataset. National Geo-Spatial Information Division, DRDLR. URL: https://ngi.dalrrd.gov.za/index.php/what-we-do/aerial-photography-and-imagery/35-colour-digital-aerial-imagery-at-0-5m-gsd-2008-2016-and-0-25m-gsd-2017-current

COLE P (2024) PyGMI – a python package for geoscience modelling and interpretation. *J. Open-Source Softw.* **10** (111) 7019. https://doi.org/10.21105/joss.07019

ÇORBACIOĞLU ŞK and AKSEL G (2023) Receiver operating characteristic curve analysis in diagnostic accuracy studies: A guide to interpreting the area under the curve value. *Turk. J. Emerg. Med.* **23** (4) 195–198. https://doi.org/10.4103/tjem.tjem_182_23

COUNCIL FOR GEOSCIENCE (2019) *Republic of South Africa 1:1 million scale Geological Map*. URL: https://www.geoscience.org.za/cgs/systems/publications/downloadable-material/ (Accessed 20 January 2023).

DAR T, RAI N and BHAT A (2020) Delineation of potential groundwater recharge zones using analytical hierarchy process (AHP). *Geol. Ecol. Landscapes* **5** (4) 292–307. https://doi.org/10.1080/24749508.2020.1726562

DEA (Department of Environmental Affairs, South Africa) (2018) South African National Land Cover (SANLC) Data. Department of Environmental Affairs, Pretoria. URL: https://www.environment.gov.za/projectsprogrammes/egis_landcover_datasets (Accessed 10 January 2025)

DE BEER CH (1990) Simultaneous folding in the western and southern branches of the Cape Fold Belt. *S. Afr. J. Geol.* **93** (4) 583–591.

DE BEER CH (1995) Fold interference from simultaneous shortening in different directions: The Cape Fold Belt syntaxis. *J. Afr. Earth Sci.* **21** (1) 157–169. https://doi.org/10.1016/0899-5362(95)00084-7

DE BEER CH (1999) Structure of the Cape fold belt in the Ceres Arc. *Council Geosci. Bull.* **123** 93 pp.

DE VILLIERS J (1960) The manganese deposits of the Union of South Africa. *Geological Survey of South Africa, Handbook 2*. Government Printer, Pretoria. 280 pp.

DHANSAY T (2021) Shattered crust: how brittle deformation enables Critical Zone processes beneath southern Africa. *S. Afr. J. Geol.* **124** (2) 519–536. https://doi.org/10.25131/sajg.124.0044

DÍAZ-ALCAIDE S and MARTÍNEZ-SANTOS P (2019) Review: advances in groundwater potential mapping. *Hydrogeol. J.* **27** (7) 2307–2324. https://doi.org/10.1007/s10040-019-02001-3

DUGUMA TA and DUGUMA GA (2022) Assessment of groundwater potential zones of upper Blue Nile River Basin using multi-influencing factors under GIS and RS environment: a case study on Guder Watersheds, Abay Basin, Oromia Region, Ethiopia. *Geofluids* **2022** 1172039. https://doi.org/10.1155/2022/1172039

EMBABY A, YOUSSEF YM and ABU EL-MAGD SA (2024) Delineation of lineaments for groundwater prospecting in hard rocks: inferences from remote sensing and geophysical data. *Environ. Earth Sci.* **83** (2) 1–28. https://doi.org/10.1007/s12665-023-11389-x

EARTH RESOURCES OBSERVATION AND SCIENCE (EROS) CENTER (2020) Landsat 8-9 Operational Land Imager / Thermal Infrared Sensor Level-2, Collection 2 [dataset]. United States Geological Survey. URL: https://doi.org/10.5066/P9OGBGM6

EUROPEAN SPACE AGENCY (ESA) (2019) URL: https://sentinel.esa.int/web/sentinel/missions/sentinel-2 (Accessed 19 August 2019).

FUNK C, PETERSON P, LANDSFELD M, PEDREROS D, VERDIN J, SHUKLA S and MICHAELSEN J (2015) The climate hazards infrared precipitation with stations – a new environmental record for monitoring extremes. *Sci. Data* **2** (1) 150066. https://doi.org/10.1038/sdata.2015.66

GISGEOGRAPHY (2015) 10 open source remote sensing software packages. URL: https://gisgeography.com/open-source-remote-sensing-software-packages/ (Accessed December 23, 2015).

GREENCAPE (2019) Using groundwater: options for managing saline wastewater/brine. URL: https://www.greencape.co.za/assets/Uploads/Brine-Industry-Brief-WEB-12-4-2019.pdf (Accessed 6 September 2020).

GUDURU JU and JILO NB (2022) Groundwater potential zone assessment using integrated analytical hierarchy process-geospatial driven in a GIS environment in Gobele watershed, Wabe Shebele river basin, Ethiopia. *J. Hydrol. Region. Stud.* **44** 101218. https://doi.org/10.1016/j.ejrh.2022.101218

GULBET TEBEGE E, MOLLA BIRARA Z, GETAHUN TAKELE S and JOTHIMANI M (2025) Geospatial mapping and multi-criteria analysis of groundwater potential in Libo Kemkem watershed, upper blue Nile River basin, Ethiopia. *Sci. Afr.* **27** e02549. https://doi.org/10.1016/j.sciaf.2025.e02549

GURU B, SESHAN K and BERA S (2017) Frequency ratio model for groundwater potential mapping and its sustainable management in cold desert, India. *J. King Saud Univ. Sci.* **29** (3) 333–347. https://doi.org/10.1016/j.jksus.2016.08.003

HAGEN A (2002) Multi-method assessment of map similarity. In: *Proceedings of the 5th AGILE Conference on Geographic Information Science, European Commission*, 25–27 April, 2002, Palma, 171–182.

HAGENLOCHER M, MEZA I, ANDERSON CC, MIN A, RENAUD FG, WALZ Y, SIEBERT S and SEBESVARI Z (2019) Drought vulnerability and risk assessments: state of the art, persistent gaps, and research agenda. *Environ. Res. Lett.* **14**. https://doi.org/10.1088/1748-9326/ab225d

HÄLBICH IW (1992) The Cape Fold Belt orogeny: State of the art 1970's–1980's. In: De Wit MJ and Ransome IGD (eds.) *Inversion Tectonics of the Cape Fold Belt, Karoo and Cretaceous Basins of Southern Africa*. Balkema, Rotterdam. 141–158.

HEIDBACH O, RAJABI M, CUI X, FUCHS K, MÜLLER B, REINECKER J, REITER K, TINGAY M, WENZEL F, XIE F and ZIEGLER MO (2018) The World Stress Map database release 2016: Crustal stress pattern across scales. *Tectonophysics* **744** 484–498. https://doi.org/10.1016/j.tecto.2018.07.007

ISHOLA KS, FATOYINBO AA, HAMID-MOSAKU AI, OKOLIE CJ, DARAMOLA OE and LAWAL TO (2023) Groundwater potential mapping in hard rock terrain using remote sensing, geospatial and aeromagnetic data. *Geosyst. Geoenviron.* **2** (1) 1–19. https://doi.org/10.1016/j.geogeo.2022.100107

JAPAN AEROSPACE EXPLORATION AGENCY EARTH OBSERVATION RESEARCH CENTER (JAXA EORC) (2025) Global 25 m Resolution PALSAR-2/PALSAR Mosaic (Ver.2.5.0) dataset description. URL: https://www.eorc.jaxa.jp/ALOS/en/dataset/pdf/DatasetDescription_PALSAR2_Mosaic_ver250.pdf (Accessed 15 May 2025).

JIA H and LIN L (2010) Optimisation of representative elementary area (REA) for the preparation of lineament density map of fractured rock aquifer. *Water SA* **36** (3) 295–308.

KABETO J, ADEBA D, REGASA MS and LETA MK (2022) Groundwater potential assessment using GIS and remote sensing techniques: case study of West Arsi Zone, Ethiopia. *Water* **14** 1838. https://doi.org/10.3390/w14121838

KAMARAJ P, JOTHIMANI M, PANDA B and SABARATHINAM C (2023) Mapping of groundwater potential zones by integrating remote sensing, geophysics, GIS, and AHP in a hard rock terrain. *Urb. Clim.* **51** 1–17. https://doi.org/10.1016/j.uclim.2023.101610

KHAN MYA, ELKASHOUTY M and TIAN F (2022) Mapping groundwater potential zones using analytical hierarchical process and multicriteria evaluation in the Central Eastern Desert, Egypt. *Water* **14** 1041. https://doi.org/10.3390/w14071041

KILLICK AM (2020) The setting and style of manganese mineralization in the Constantiaberg Massif, Cape Peninsula, South Africa. *S. Afr. J. Geol.* **123** (4) 493–510. https://doi.org/10.25131/sajg.123.0034

LATUNDE T and BAMIGBOLA OM (2018) Parameter estimation and sensitivity analysis of an optimal control model for capital asset management. *Adv. Fuzzy Syst.* **2018** (1) 4756520. https://doi.org/10.1155/2018/4756520

LEE S, HYUN Y and LEE MJ (2019) Groundwater potential mapping using data mining models of big data analysis in Goyang-si, South Korea. *Sustainability* **11** (6) 1–21. https://doi.org/10.3390/su11061678

LIN L, LIN H, XU Y, NTULI T and MAHLANGU F (2015) Impact of fault structures on the occurrence of groundwater in fractured rock aquifers. WRC Report No. 2053/1/14. Water Research Commission, Pretoria.

MACHARIS C, SPRINGAEL J, De BRUCKER K and VERBEKE A (2004) Promethee and AHP: The design of operational synergies in multicriteria analysis. Strengthening Promethee with ideas of AHP. *Eur. J. Oper. Res.* **153** 307–317. https://doi.org/10.1016/S0377-2217(03)00153-X

MALCZEWSKI J (2006) GIS-based multicriteria decision analysis: a survey of the literature. *Int. J. Geogr. Inf. Sci.* **20** (7) 703–726. https://doi.org/10.1080/13658810600661508

MANZUNZU B, MIDZI V, MULABISANA TF, ZULU B, PULE T, MYENDEKI S and RATHOD GW (2019) Seismotectonics of South Africa. *J. Afr. Earth Sci.* **149** 271–279. https://doi.org/10.1016/j.jafrearsci.2018.08.012

MARCHANT JW, WILLIS JP and DUNCAN AR (1978) Geochemistry of the Table Mountain Group, 1: Aspects of the origin of the Houtbaai manganese deposit. *Trans. Geol. Soc. S. Afr.* **81** 179–184.

MEYER PS (2001) *1:500 000 Hydrogeological Map Series of Cape Town 3317.* Department of Water Affairs and Forestry, Pretoria.

MORGAN H, HUSSIEN HM, MADANI A and NASSAR T (2022) Delineating groundwater potential zones in hyper-arid regions using the applications of remote sensing and GIS modeling in the Eastern Desert, Egypt. *Sustainability* **14** (24) 1–30. https://doi.org/10.3390/su142416942

MUKHAWANA MB, KANYERERE T, KAHLER D, MASILELA NS, LALUMBE L and UMUNEZERO AA (2024) Hydrological drought assessment using the standardized groundwater index and the standardized precipitation index in the Berg River Catchment, South Africa. *J. Hydrol. Region. Stud.* **53** 1–17. https://doi.org/10.1016/j.ejrh.2024.101779

NAINGGOLAN L, NI CF, DARMAWAN Y, LO WC, LEE IH, LIN, CP and HIEP NH (2024) Cost-effective groundwater potential mapping by integrating multiple remote sensing data and the index–overlay method. *Remote Sens.* **16** (3) 502. https://doi.org/10.3390/rs16030502

NASA JPL (National Aeronautics and Space Administration Jet Propulsion Laboratory) (2013) NASA Shuttle Radar Topography Mission Global 1 arc second. In: *NASA EOSDIS Land Processes Distributed Active Archive Center.* https://doi.org/10.5067/MEaSUREs/SRTM/SRTMGL1.003

NEWTON AR (1993) The Cape folding-a syntaxis or not? *S. Afr. J. Geol.* **96** 213–215.

NEWTON AR, SHONE RW and BOOTH PWK (2006) The Cape Fold Belt. In: Johnson MR, Anhaeusser CR and Thomas RJ (eds) *The Geology of South Africa.* Geological Survey of South Africa, Johannesburg/Council for Geoscience, Pretoria. 521–528.

OWOLABI ST, MADI K and KALUMBA AM (2020) A groundwater potential zone mapping approach for semi-arid environments using remote sensing (RS), geographic information system (GIS), and analytical hierarchical process (AHP) techniques: a case study of Buffalo catchment, Eastern Cape, South Africa. *Arab. J. Geosci.* **13** 1184. https://doi.org/10.1007/s12517-020-06166-0

PATEL DK, THAKUR TK, THAKUR A, KARUPPANNAN S, SWAMY SL and PANT RR (2024) Groundwater potential zone mapping using AHP and geospatial techniques in the upper Narmada basin, central India. *Discover Sustain.* **5** (1) 355. https://doi.org/10.1007/s43621-024-00560-4

PRIYA U, IQBAL MA, SALAM MA, NUR-E-ALAM M, UDDIN MF, ISLAM ARMT, SARKAR SK, IMRAN SI and RAK AE (2022) Sustainable groundwater potential zoning with integrating GIS, remote sensing, and AHP model: A case from north-central Bangladesh. *Sustainability* **14** (9) 1–24. https://doi.org/10.3390/su14095640

QADIR J, BHAT MS, ALAM A and RASHID I (2020) Mapping groundwater potential zones using remote sensing and GIS approach in Jammu Himalaya, Jammu and Kashmir. *GeoJournal* **85** 487–504. https://doi.org/10.1007/s10708-019-09981-5

RESEARCH INSTITUTE FOR KNOWLEDGE SYSTEMS (RIKS BV) (2010) Map comparison kit version 3.2.1.: User manual. URL: http://www.riks.nl/products/Map-Comparison-Kit (Accessed 10 May 2025).

SALAKO ADEBAYO O and ADEPELUMI ABRAHAM A (2018) Aquifer, classification and characterization. In: Javaid MS and Khan SA (eds) *Aquifers – Matrix and Fluids.* IntechOpen. https://doi.org/10.5772/intechopen.72692

SHANDU ID and ATIF I (2023) An integration of geospatial modelling and machine learning techniques for mapping groundwater potential zones in Nelson Mandela Bay, South Africa. *Water* **15** (19) 3447. https://doi.org/10.3390/w15193447

SARAVANAN S, SARANYA T, ABIJITH D, JACINTH JJ and SINGH L (2021) Delineation of groundwater potential zones for Arkavathi sub-watershed, Karnataka, India using remote sensing and GIS. *Environ. Challenges.* **5** 1–16. https://doi.org/10.1016/j.envc.2021.100380

ŞENER E, ŞENER Ş and DAVRAZ A (2018) Groundwater potential mapping by combining fuzzy-analytic hierarchy process and GIS in Beyşehir Lake Basin, Turkey. *Arab. J. Geosci.* **11** https://doi.org/10.1007/s12517-018-3510-x

SHABAN A, EL-BAZ F and KHAWLIE M (2007) The relation between water-wells productivity and lineaments morphometry: selected zones from Lebanon. *Hydrol. Res.* **38** (2) 187–201. https://doi.org/10.2166/nh.2007.007

SCHOBER P, BOER C and SCHWARTE LA (2018) Correlation coefficients: appropriate use and interpretation. *Anesthesia Analgesia* **126** (5). URL: https://journals.lww.com/anesthesia-analgesia/fulltext/2018/05000/correlation_coefficients__appropriate_use_and.50.aspx

SHEBL A, ABDELAZIZ MI, GHAZALA H, ARAFFA SAS, ABDELLATIF M and CSÁMER Á (2022) Multi-criteria groundwater potentiality mapping utilizing remote sensing and geophysical data: A case study within Sinai Peninsula, Egypt. *Egypt. J. Remote Sens. Space Sci.* **25** (3) 765–778. https://doi.org/10.1016/j.ejrs.2022.07.002

SMIDA H, DASSI L, BOUKHACHEM K and MASROUHI A (2022) Satellite remote sensing and GIS-based multi-criteria analysis for the assessment of groundwater potentiality in fractured limestone aquifer: Case study of Maknassy Basin, central Tunisia. *J. Afr. Earth Sci.* **195** 1–25. https://doi.org/10.1016/j.jafrearsci.2022.104643

SOUTH AFRICAN NATIONAL SPACE AGENCY (SANSA) (2022) SPOT 6 and SPOT 7 imagery now available at SANSA. URL: https://www.sansa.org.za/2015/07/01/sansa-spot-imagery/ (Accessed 6 June 2020).

STELLENBOSCH MUNICIPALITY (2024) 5th Generation Integrated Development Plan (IDP 2022–2027). 2nd review. URL: https://stellenbosch.gov.za/download/final-adopted-2nd-review-of-the-5th-generation-idp-2022-2027-may-2024/?ind=1717411139759&filename=5th-Generation-Integrated-Development-Plan-2022-2027-v38.pdf&wpdmdl=24580&refresh=68be954ed1ef31757320526 (Accessed 8 September 2025).

TAMESGEN Y, ATLABACHEW A and JOTHIMANI M (2023) Groundwater potential assessment in the Blue Nile River catchment, Ethiopia, using geospatial and multi-criteria decision-making techniques. *Heliyon* **9** (6) e17616. https://doi.org/10.1016/j.heliyon.2023.e17616

TESSEMA A, MENGISTU H, CHIRENJE E, ABIYE T and DEMLIE M (2011) The relationship between lineaments and borehole yield in North West Province, South Africa: Results from geophysical studies. *Hydrogeol. J.* **20** (2). https://doi.org/10.1007/s10040-011-0803-5

THAMAGA KH, GOM S, ADESOLA GO, NDOU N, MUAVHI N, MNDELA M, SIBANDZE P, GHASSAN ABDO N, MAPHANGA T, ABAYOMI AFUYE G and co-authors (2024) Integration of geospatial-based algorithms for groundwater potential characterization in Keiskamma Catchment of South Africa. *Groundwater Sustain. Dev.* **26** 101262. https://doi.org/10.1016/j.gsd.2024.101262

THANH NN, THUNYAWATCHARAKUL P, NGU NH and CHOTPANTARAT S (2022) Global review of groundwater potential models in the last decade: parameters, model techniques, and validation. *J. Hydrol.* **614** (Part A) 128501. https://doi.org/10.1016/j.jhydrol.2022.128501

THAPA R, GUPTA S, GUIN S and KAUR H (2018) Sensitivity analysis and mapping the potential groundwater vulnerability zones in Birbhum district, India: A comparative approach between vulnerability models. *Water Sci.* **32** 44–66. https://doi.org/10.1016/j.wsj.2018.02.003

THERON JN, GRESSE PG, SIEGFRIED HP and ROGERS J (1992) *The geology of the Cape Town area. Explanation Sheet 3318 (1:250 000).* Geological Survey of South Africa. 140 pp.

UPWANSHI M, DAMRY K, PATHAK D, TIKLE S and DAS S (2023) Delineation of potential groundwater recharge zones using remote sensing, GIS, and AHP approaches. *Urb. Clim.* **48** 1–12. https://doi.org/10.2139/ssrn.4170691

VAN ENGELEN VWP and DIJKSHOORN JA (2012) Global and national Soils and Terrain Digital Databases (SOTER) procedures manual. URL: http://www.isric.org (Accessed 12 November 2024).

XU L, LIN L and JIA H (2009) Groundwater flow conceptualization and storage determination of the Table Mountain Group (TMG) aquifers. WRC Report No. 1419/1/09. Water Research Commission, Pretoria. 268 pp.

ZHU Q and ABDELKAREEM M (2021) Mapping groundwater potential zones using a knowledge-driven approach and GIS analysis. *Water* **13** (5) 579. https://doi.org/10.3390/w13050579